Nanoscale

PAPER

View Article Online
View Journal | View Issue

Cite this: *Nanoscale*, 2015, **7**, 5843

Synthesis and thermal behavior of tin-based alloy (Sn–Ag–Cu) nanoparticles†

Ali Roshanghias,*[a] Andriy Yakymovych,[a] Johannes Bernardi[b] and Herbert Ipser[a]

Received 21st January 2015,
Accepted 23rd February 2015

DOI: 10.1039/c5nr00462d

www.rsc.org/nanoscale

The prominent melting point depression of nanoparticles has been the subject of a considerable amount of research. For their promising applications in electronics, tin-based nano-alloys such as near-eutectic Sn–Ag–Cu (SAC) alloys have been synthesized *via* various techniques. However, due to issues such as particle aggregation and oxidation or introduced impurities, the application of these nano-size particles has been confined or aborted. For instance, thermal investigations by DTA/DSC in a large number of studies revealed exothermic peaks in the range of 240–500 °C, *i.e.* above the melting point of SAC nanoparticles, with different and quite controversial explanations for this unclear phenomenon. This represents a considerable drawback for the application of nanoparticles. Correspondingly, in the current study, the thermal stability of SAC nanoparticles has been investigated *via* electron microscopy, XRD, FTIR, and DSC/TG analysis. It was found that the nanoparticles consist mainly of a metallic β-Sn core and an amorphous tin hydroxide shell structure. The SnO crystalline phase formation from this amorphous shell has been associated with the exothermic peaks on the first heating cycle of the nanoparticles, followed by a disproportionation reaction into metallic Sn and SnO_2.The results also revealed that the surfactant and reducing agent cannot only affect the size and size distribution of the nanoparticles, they might also alter the ratio between the amorphous shell and the crystalline core in the structure of particles.

Introduction

Nanostructured materials have attracted considerable interest due to their unique properties and their potential for numerous industrial applications. Various fundamental physical properties such as the melting point have been theoretically predicted and empirically proven to change as the material size decreases.[1,2] Due to the importance of this nano-size effect in electronic materials, tin and tin-based nanoalloys have been synthesized and studied recently as possible solder materials.[2–5] However, their potent reactivity with respect to water and oxygen, along with a high surface-area to volume ratio favors an easy oxidation. Furthermore, the tendency to agglomerate leads to a decrease of the nanoparticles' activity, thereby reducing the nano-size effect or even eliminating it entirely. Investigations on the thermal performance of many tin-based nanomaterials revealed unexpected emissions of energy represented by exothermic peaks on the first heating curves in DTA (differential thermal analysis) or DSC (differential scanning calorimetry). Not only have these exothermic peaks never been reported for tin as a bulk material, they also disappeared in the consequent heating cycles of the nanoparticles. Whilst some authors ascribed this phenomenon to the oxidation of Sn nanoparticles, others attributed it to either decomposition of organic residues and burning of the surfactant or to a partial coalescence of nano-clusters and aggregation.[5–9]

In fact, this exothermal effect appears to have a complex nature and might involve several different processes. Exothermic peaks were also reported for other nanomaterials, as for example nano-$CoSn_3$,[10] nano-$Co_3Sn_3C_4$ (actually nano-CoSn in a carbon matrix)[11] and nano-$FeSn_2$.[12] In a similar investigation, Prasad and Chokshi[13] studied the exothermic peak during annealing of electrodeposited nanocrystalline nickel, which was associated with the formation of a nickel sulfide (Ni_3S_2) phase and the subsequent accelerated grain growth.

The knowledge on the conditions for the preparation of tin-based nanoparticles must go along with an understanding of their thermal stability and oxidation mechanisms. Song and Wen[14] extensively investigated the oxidation of tin nanoparticles and identified a two stage oxidation process of tin accompanied by two exothermic peaks: formation of the monoxide SnO below 400 °C and the transformation of SnO into the dioxide SnO_2 at a higher temperature. On the other hand, many studies focused on the synthesis of pure Sn,[2,7,9] near-eutectic Sn–Ag (SA)[1,8] and Sn–Ag–Cu (SAC)[5,6,15–18] nanoparticles

[a]*Department of Inorganic Chemistry (Materials Chemistry), University of Vienna, A-1090 Vienna, Austria. E-mail: Ali.roshanghias@univie.ac.at*
[b]*Vienna University of Technology, USTEM, A-1040 Vienna, Austria*
† Dedicated to Prof. Brigitte Weiss.

as promising candidates for the next generation of lead-free solders due to their reduced melting temperature.

In fact, melting point depression in nanosolders was the main interest of most of these investigations, since the melting point of the eutectic SAC bulk alloys is 217 °C, about 34 °C higher than that of the conventional Sn–Pb solders.[15] However, this target was not readily approachable in some of these research studies. For instance, Hsiao and Duh[5] observed no obvious melting point depression in their SAC nanoparticles, whereas Jiang *et al.*[4] reduced the melting point by up to 20 °C by employing a surfactant agent. Due to the capping effect caused by the surfactant molecules' coordination with the nanoclusters, surfactants are believed to suppress particle growth and protect the particle surface from oxidation.

Although the decrease of the melting temperature of solder nanoparticles has been studied repeatedly the thermal stability of eutectic or near-eutectic SAC nanoparticles has rarely been studied over the entire temperature range. In particular, to the best of our knowledge, the appearance of an exothermic peak in the DSC/DTA heating curves above the melting temperature of SAC alloys has been either overlooked or not investigated more closely in the previous studies. Unfortunately, in most of the cases either the DSC scanning range was restricted to the melting range of SAC alloys or the DSC curves have been cut-out or magnified, demonstrating only the melting region, ignoring all the possible reactions before and after the melting of the metallic SAC particles. Only in very few studies, some hints and evidence of these exothermic peaks have been implied. For instance, Sopousek *et al.*[8] reported a 4.3 °C melting depression for 90 nm Sn–Ag nanoparticles followed by an exothermal effect between 230 and 270 °C only in the first heating cycle. Moreover, in many cases the nanoparticles frequently turned into micro-size powders rather than bulk spheres after heat treatment, which implies an impurity contribution due to the surfactant and shows that surfactants may be difficult to remove.[8] Jiang *et al.*[4] attributed the observed weight loss below the melting point of the nanoparticles to the evaporation and/or decomposition of absorbed moisture and surfactants and the weight gain above the melting point to thermal oxidation of the Sn or SAC alloy nanoparticles.

Gao *et al.*[16] prepared SAC nanoparticles in the range of 15–60 nm with an average of about 30 nm. Although the DSC heating curves were confined to the region from 150 to 230 °C, namely below the exothermic peak appearance, the existence of a superficial oxide layer has been implicitly suggested.

To address these issues regarding thermal stability and performance of nanoparticles, near-eutectic SAC nanoparticles have been synthesized in this study *via* chemical reduction and a systematic investigation on the phase evolution upon DSC heating of the as-synthesized nanoparticles has been carried out. Chemical reduction of metallic cations by a strong reducing agent is an interesting route to obtain alloy nanoparticles, because it is quick, efficient and suitable for industrial manufacture. Consequently, the morphology, microstructure and thermal behavior of the as-synthesized powder have been investigated up to 650 °C.

Experimental procedure

Tin-based, near eutectic (Sn-3.8 wt% Ag-0.7 wt% Cu) nano powder alloys have been synthesized *via* a chemical reduction technique by employing sodium borohydride ($NaBH_4$; Alfa-Aesar) and polyvinylpyrrolidone (PVP; Alfa-Aesar) as the reducing agent and surfactant agent, respectively. Correspondingly, stoichiometric amounts of tin(II) 2-ethylhexanoate ($C_{16}H_{30}O_4Sn$; Alfa-Aesar) and silver nitrate ($AgNO_3$; Merck) and copper(II) nitrate trihydrate ($Cu(NO_3)_2{\cdot}3H_2O$; Merck) were dissolved in diethylene glycol (DEG; Alfa-Aesar) as the metal precursors. PVP and $NaBH_4$ were dissolved separately in DEG and rapidly added to solutions of the metal precursors under rapid stirring for 1 h. The amount of $NaBH_4$ varied from zero to 8 times the molar ratio of the SAC powder, for a typical 1 g metallic powder synthesis. Analogously, various molar ratios of PVP to SAC ($n_{PVP}/n_{SAC} \leq 1$) were added to the solution to control the morphology and size distribution of the powders. For the sake of simplicity, from now on nanoparticles will be denoted as N_xP_y where x and y are the molar ratios of $NaBH_4$ and PVP to SAC nanopowders, respectively.

After the reaction was complete, the obtained precipitates were separated from the organic residue by centrifugation at 4000 rpm for 30 min, rinsed several times with a large amount of absolute ethanol to remove the excess amount of surfactants, filtered and finally dried in a vacuum for one day at room temperature.

For particle size analysis, the nanoparticles were dispersed in ethanol, and a drop of this dispersion was trickled on a polished Si wafer for scanning electron microscopy (SEM) or on a copper grid coated with a carbon film for transmission electron microscopy (TEM) investigations. SEM studies were performed on a scanning electron microscope (Zeiss Supra 55 ESEM). TEM investigations were made by utilizing a (FEI TECNAI F20 TEM) microscope equipped with energy-dispersive spectroscopy (EDS) and energy-loss spectroscopy (EELS). Elemental analysis for carbon, hydrogen and nitrogen was also performed using a Perkin Elmer C/H/N elemental analyzer.

X-ray diffraction (XRD) patterns were obtained on a D8 Advance X-ray diffractometer (Bruker). Rietveld refinements were performed with the Topas 3 software by which the average crystallite size, the amount of crystallinity and weight percentages of phases were obtained. For thermogravimetry (TG) and differential scanning calorimetry (DSC) a TG-DSC instrument (Labsys, SETARAM, Lyon) was used and experiments were carried out over the temperature range from room temperature to 650 °C at a heating rate of 5 K min^{-1} under the flow of Ar gas. Complementary information on powder morphology was obtained using Fourier transform infrared spectroscopy (FTIR) in the spectral range 4000–400 cm^{-1}.

Results and discussion

Structure and morphology

Fig. 1a, b and d exhibit the SEM images and particle size distribution of the as-synthesized nanoparticles. It shows that PVP

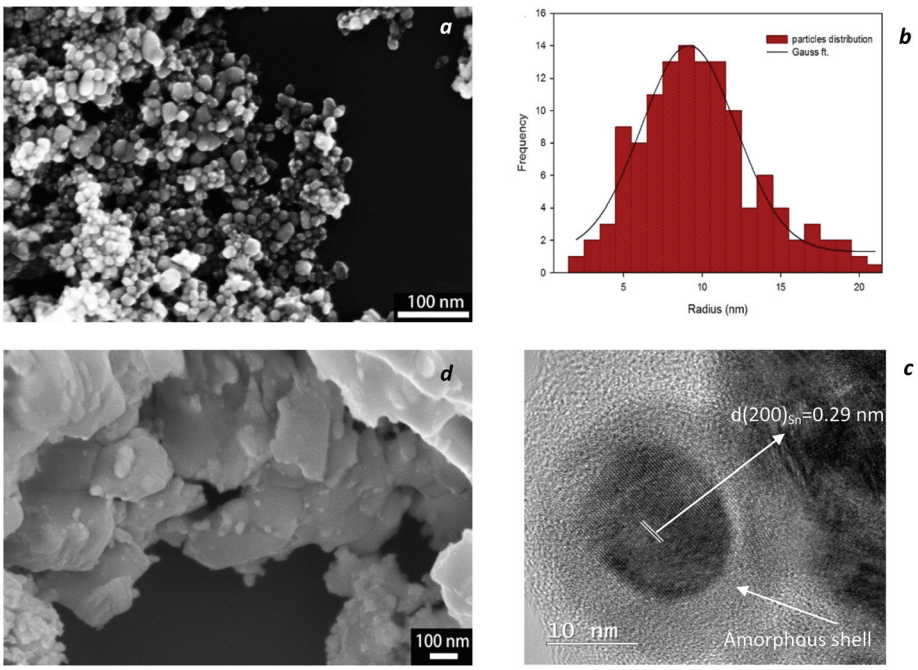

Fig. 1 SEM image of as-synthesized SAC particles with (a) and without (d) the use of a surfactant (PVP). A size distribution histogram of the particles in (a) is presented in (b). The HRTEM image of a nanoparticle from (a) is shown in (c) which consists of a well-crystallized β-Sn core of *ca.* 18 nm diameter covered with an amorphous layer of *ca.* 5 nm.

has a significant influence on the size and the morphology of the nanoparticles. Without PVP, the nuclei and nanocrystals of SAC alloy tend to merge into large facet-like particles *via* agglomeration (Fig. 1d). In contrast, the use of PVP leads to nano-size spherical particles with a narrow size distribution as shown in Fig. 1a–c. Fig. 2 shows a plot of the average particle size of the nanoparticles as a function of surfactant concentration. It was found that by introducing PVP to the precursors, particle size decreased drastically, while a further increase in the amount of PVP altered the particle size only slightly, which is probably due to the fact that the surface of the particles becomes saturated by the surfactant molecules.

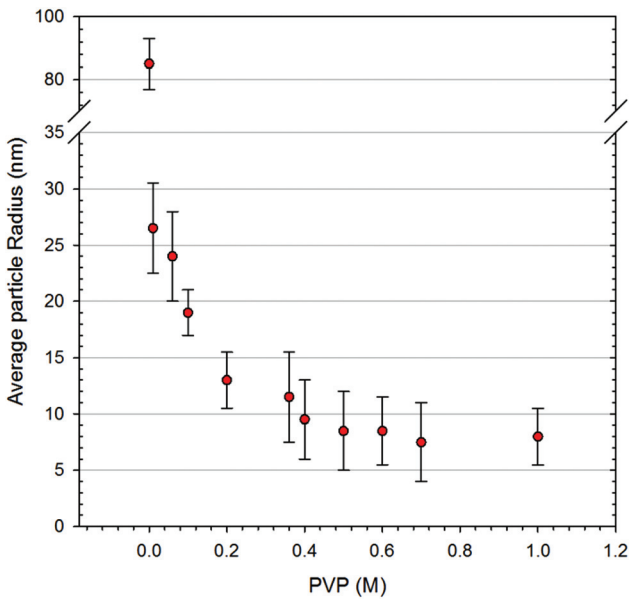

Fig. 2 The effect of PVP concentration on the average particle size (*r*) of nanoparticles.

According to the phase diagram,[19] near-eutectic ternary SAC alloys contain three phases at room temperature with the corresponding weight percentages: β-Sn (93 wt%), Ag_3Sn (5.2 wt%) and Cu_6Sn_5 (1.8 wt%). All XRD patterns of the synthesized nanopowders at room temperature could be readily indexed to the tetragonal phase of β-Sn and orthorhombic Ag_3Sn. The formation of the Ag_3Sn intermetallic compound indicates successful alloying *via* the chemical co-reduction process. The third constituent, Cu_6Sn_5, was detected only after heat treatment up to 650 °C as highlighted in Fig. 3b. Apparently, the amount of crystalline Cu_6Sn_5 was not sufficient to reveal the XRD pattern at room temperature, however, at higher temperatures and with the corresponding increase in crystallinity, Cu_6Sn_5 was also identified.

Moreover, from the XRD patterns, no obvious oxidation peaks were found at room temperature, even though no surfactant was applied to some of the samples. Nonetheless, the high-resolution TEM image in Fig. 1c clearly shows that the surface of the particles appears to be covered by an amorphous layer since a long range ordering of lattice planes is not observed in this outer layer. The interplanar spacing of the lattice fringes in the core of the particle was measured and found to be approximately 0.29 nm; this value corresponds to

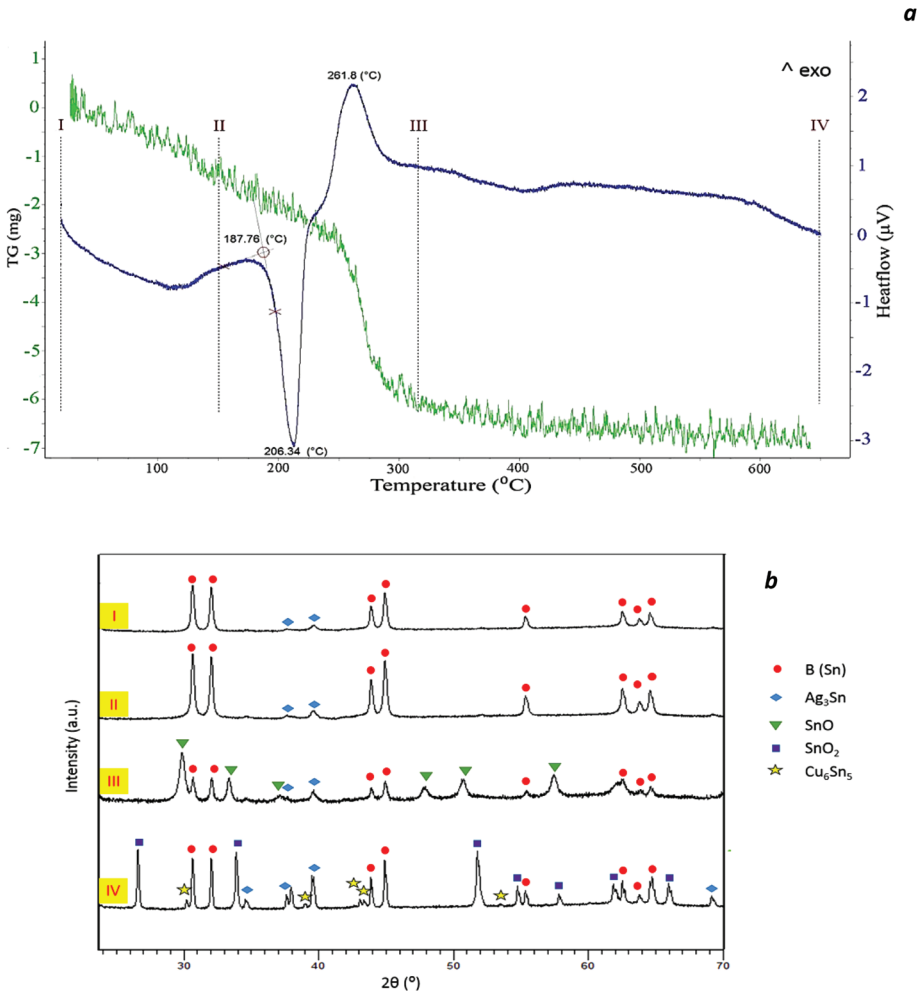

Fig. 3 DSC/TG curves of ($N_6P_{0.4}$) Sn–Ag–Cu nanoparticles (a) and the corresponding XRD patterns (b) of a sample at room temperature (I), heated up to 150 °C (II), 320 °C (III) and 650 °C (IV).

that of the {200} planes of a tetragonal β-Sn crystal. A similar core–shell structure for tin-based nanoparticles has been frequently reported; whilst some authors believed that the amorphous shell is in fact the surfactant, *i.e.* phenanthroline[20] or PVP,[15] others specified this layer as amorphous SnO_x [7,21] as well as crystalline defects such as kinks and ledges on the particle surface.[6]

EDS and EELS analyses revealed that the surface of the nanoparticles was enriched with Sn and O. Moreover, chemical CHN analysis proved that the as-synthesized product contained to some extent C and H. Thus, it can be postulated that the shell consisted in fact of two approximately co-axial sublayers; an amorphous tin oxide layer around the β-Sn core as well as an amorphous hydroxide layer entangled with polar PVP groups, which will be discussed later. The presence of noticeable amounts of tin hydroxide can be easily explained by the fact that the reducing $NaBH_4$ solution reacts basic and Sn^{2+} ions are precipitated as an ill-defined hydroxide $SnO{\cdot}xH_2O$ ("$Sn(OH)_2$") in basic solutions.[22] Even though the synthesis was performed in non-aqueous solvents, the water content introduced with the solvent DEG, with PVP and the solid precursor salts was apparently high enough to provide the necessary hydroxide groups, as seen from Fig. 4.

Fig. 4 displays the FT-IR spectrum of a sample of as-synthesized nanoparticles using PVP in the reduction process. As inferred from the characteristic bands in this figure, the intensive and broad band around 3200 cm^{-1} corresponds to the O–H vibrations, which are most probably due to the hydroxyl groups attached on the surface of nanoparticles. The clearly visible C=O and C–O stretching bands at about 1680 and 1150 cm^{-1}, respectively, might correspond to PVP which is coordinated and/or adsorbed to the particle surface.

Thermal behavior

Fig. 3a presents the DSC-TG curves of $N_6P_{0.4}$ nanoparticles heated up to 650 °C, which have been marked at 4 different temperatures. Fig. 3b shows the corresponding XRD patterns of a sample at room temperature and heated in the DSC apparatus up to three successively higher temperatures.

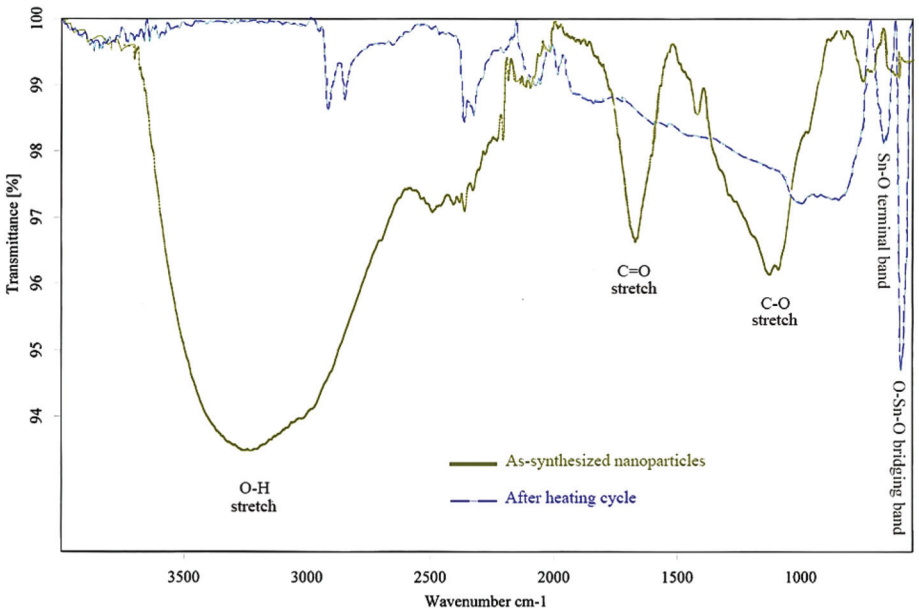

Fig. 4 The infrared spectra of as-synthesized and heat treated nanoparticles ($N_6P_{0.4}$) at 650 °C.

As seen in the DSC curve, between 80 and 120 °C a broadened endothermic peak exists which is attributed to the removal of the solvent physically adsorbed to the particles. The melting onset was evaluated as 187.8 °C, which was 26.6 °C lower than that of micron sized particles. The melting transition took place over a temperature range of about 30 °C. This phenomenon can be attributed to the broadening of the phase transition due to the finite size effect and size distribution of nanoparticles.[23,24]

A prominent exothermic peak was observed around 261 °C (peak maximum) which, according to the corresponding phase evolution in the XRD patterns of (b) and (c), could be associated with the crystallization of the SnO phase. Moreover, this exothermic peak was accompanied by a weight loss of about 8% in the TGA curve. Therefore, the assumption that the peak corresponds to external oxidation due to the presence of trace oxygen in the atmosphere of the DSC chamber can be excluded. It is concluded that the observed weight loss is due to the elimination of organic residues and of OH-groups as water. In other words, the observed exothermic signal could be an indicator of the rearrangement of the tin atoms that leads to the consolidation of the tin oxide structure and its crystallization.

In order to examine the possible effect of the PVP macromolecules on the exothermic peak and the corresponding weight loss, the thermal behavior of pure PVP dissolved in DEG is presented in Fig. 5. It is obvious that, the decomposition of PVP occurs around 420 °C. Looking again at Fig. 3a one can spot a similar although weaker endothermic peak around this temperature, indicating the presence of PVP. Consequently, one must conclude that the weight loss in the lower temperature range, *e.g.* around 260 °C as in Fig. 3a, was not merely associated with the decomposition of PVP. Hence, another explanation would be the thermal decomposition of the Sn hydroxide layer that leads to the loss of water and the formation of crystalline SnO according to the following possible chemical reactions:

$$Sn^{2+} + 2OH^- \rightarrow Sn(OH)_2 \downarrow \quad (1)$$

$$Sn(OH)_2 \rightarrow SnO_{(amorphous)} + H_2O \uparrow \quad (2)$$

$$SnO_{(amorphous)} \rightarrow SnO_{(crystalline)} + \Delta Q \uparrow \quad (3)$$

The FT-IR spectrum of the same sample after DSC measurements (Fig. 4) was also consistent with this rationale, where O–H bands were strongly diminished indicating the disappearance of the OH-groups on the surface of the particles. Moreover, the appearance of two sharp peaks at low wavenumbers (595 cm^{-1} and 667 cm^{-1}) can be attributed to the formation of tin oxides upon heating. The considerably weakened C–O bands also refer to the decomposition of PVP and all organic residue, when heated over 450 °C.

As depicted in Fig. 6, the second DSC heating cycle was always different from the first heating cycle of nanoparticles, showing only the eutectic melting of the SAC alloy at a temperature close to the ternary eutectic of a bulk alloy. In addition, the quantitative evaluation of the DSC peak revealed that the heat exchange during the melting process, in particular the latent heat of fusion (ΔH_m) in the second heating cycle was 44 mV g^{-1} although in the first cycle it was evaluated as 31 mV g^{-1}.

It is worth noting that SnO is in fact a metastable phase and decomposes at higher temperatures, even in the absence of oxygen, according to the disproportionation reaction:[14]

$$2SnO = SnO_2 + Sn \quad (4)$$

The formation of the SnO_2 phase after heating up to 650 °C was corroborated by the XRD pattern (IV) in Fig. 3b. Moreover,

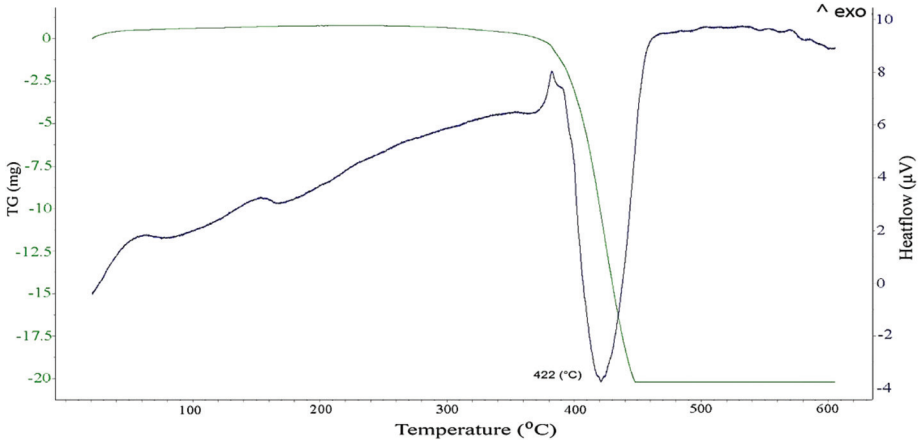

Fig. 5 DSC/TG curves of PVP dissolved in DEG.

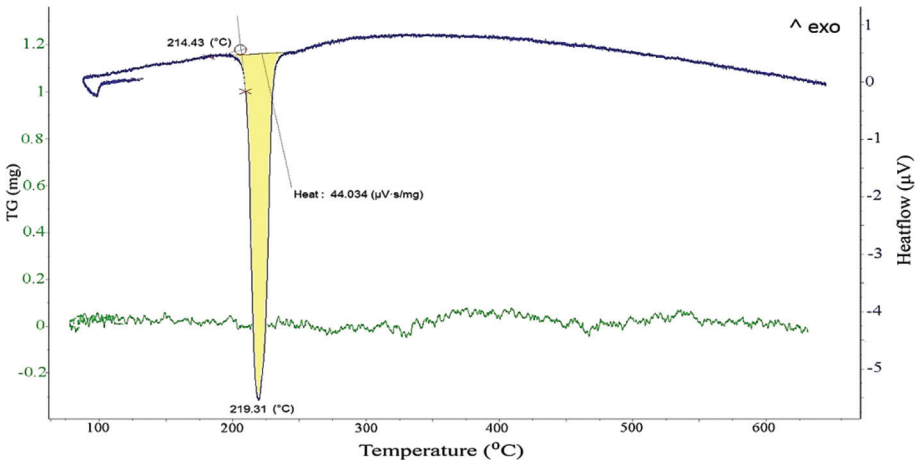

Fig. 6 DSC/TG curves of the second heating cycle of the ($N_6P_{0.4}$) Sn–Ag–Cu sample.

the intensity of the characteristic peaks of β-Sn in patterns (IV) was considerably higher than in pattern (III) which shows a clear increase in the amount of metallic Sn, anticipated by eqn (4). With this, the observed increase of 13 mV g^{-1} in the evolved heat during melting can be explained by the introduction of a new source for metallic tin as a result of the disproportionation of SnO beyond 400 °C (eqn (4)).

This amorphous surface layer may represent a major drawback for the practical use of SAC nanoparticles, prepared by chemical reduction, as reliable solders. A possible solution could be the use of an acidic soldering flux which is able to dissolve this layer. For instance, Yung *et al.*[15] removed the superficially oxidized SnO_2 layer from the SAC nanopowders by soaking in citric acid for 24 h. Jiang *et al.*[4] employed anti-oxidation agents such as butylated hydroxytoluene (BHT) or hydroquinone in the composition of the soldering paste.

Effect of PVP and $NaBH_4$

PVP has a structure of a polyvinyl skeleton with polar groups (pyrrolidone groups) and dissolves easily in DEG where it most likely adopts a pseudo-random coil conformation.[25] Although a nonionic surfactant, PVP will coordinate to the Sn^{2+} (and also to Ag^+ and Cu^{2+}) cations *via* the oxygen and nitrogen atoms in the pyrrolidone group but it will also protect the growing nanoparticles against agglomeration.[26] In the fast reaction of chemical reduction, a high number of Sn^{2+} cations are reduced to form metallic seeds, and the remaining Sn^{2+} cations will, on reduction, aggregate to these Sn seeds which will grow until all cations are used up. Without protection by the voluminous PVP molecules, the growing particles will start to agglomerate although the DEG itself will provide some coordination shell. However the presence of PVP provides excellent protection and prevents any significant sintering of the growing nanoparticles, thus controlling the size of the nanoparticles.[25–27]

On the other hand, there appears to be some competition between PVP and OH^- groups for binding sites on the surface of the growing nanoparticles, and the PVP cannot prevent the formation of "$Sn(OH)_2$" on their surface. This is clearly demonstrated by the presence of the OH band in Fig. 4. Thus it must

be concluded that the metallic nucleus of the SAC alloy is covered by a layer of more or less amorphous hydroxide and then by a protective layer of PVP, as already discussed above. The formation of an amorphous tin hydroxide gel results finally in an oxide layer during the calcination process.[28,29] On the other hand, this double layer (hydroxide and PVP) acts as a passivation layer for the nanoparticles against room temperature oxidation, as well.[3] As inferred from the FTIR spectra of the nanoparticles, O–H and C–O bonds, despite repeated washing and rinsing, exist in the structure of the obtained product, mainly due to this layer.

Of course, the protective action is not an exclusive behavior of PVP molecules. Various other surfactants, such as cetyltrimethylammoniumbromide (CTAB), polyethyleneglycol (PEG), citric acid, 1,10-phenanthroline and many others were frequently employed.[30–32] Nevertheless, PVP appears to exhibit the best protective properties among them.[25]

The amount of crystallinity for the samples synthesized with various amounts of PVP and $NaBH_4$, derived from XRD quantitative analysis, has been plotted in Fig. 7. As observed, the introduction of surfactants to the samples affects significantly the ratio of metallic crystalline phases and the amorphous portion. An increase in the concentration of $NaBH_4$ in the presence of PVP clearly promotes the reduction of metallic nanoparticles. With low concentrations of $NaBH_4$, the reduction rate of the metallic ions is low and only a small amount of nuclei is generated during the nucleation step. Thus, a large portion of the metallic ions in solution will remain suspended, prone to bind with polymeric groups and hydroxide ions. This leads to the formation of particles with a dominating amorphous layer and a dwindling metallic core. In contrast, with increasing amounts of $NaBH_4$, more BH_4^- ions are available for transferring electrons to the metallic ions.[15,30] Thus, a large number of nuclei are formed in the solution which will consume a large portion of the metallic ions. As inferred from Fig. 7, the crystallinity of the particles improved with an increase in the amount of $NaBH_4$.

However, for higher concentrations of $NaBH_4$, sodium was detected on the surface of the particles that could be attributed to the formation of a reaction by-product, $NaB(OR)_4$:[33]

$$NaBH_4 + 4ROH \rightarrow NaB(OR)_4 \downarrow + 4H_2 \uparrow \quad (5)$$

Finally, Fig. 8a, shows schematically the change of morphology of the nanoparticles upon heating. As discussed above, the core–shell structure of the nanoparticles, consisting of an amorphous shell and a metallic core, is the stable configuration of the particles at room temperature and remains stable even after melting of the inner metallic part as can be inferred from the tiny droplets detected by SEM after heating up to 650 °C (Fig. 8c). In another study on SAC nanoparticles by Gao *et al.*,[16] even during repeated DSC measurements, the bulk melting behavior was never observed, but the successive heating curves looked rather similar with a constantly depressed melting temperature. It can be speculated that the (rather massive) superficial oxide layer surrounding the individual particles obstructed the metallic cores of the particles from agglomeration and further coalescence after melting, thereby the nanoparticles remained nanoparticles or microparticles even after melting.

The HRTEM image (Fig. 8b) indicates that the single nanoparticles observed by SEM might be single crystals (as shown in Fig. 1c), or they might in fact be polycrystals or possibly agglomerated particles surrounded by an amorphous layer. Independent of that, after the heating cycle up to 650 °C, the samples consist of three distinctive parts, shiny metallic Sn–Ag–Cu spheres of various sizes, irregularly shaped SnO_2 particles on the surface of the spheres and carbonized black residues.

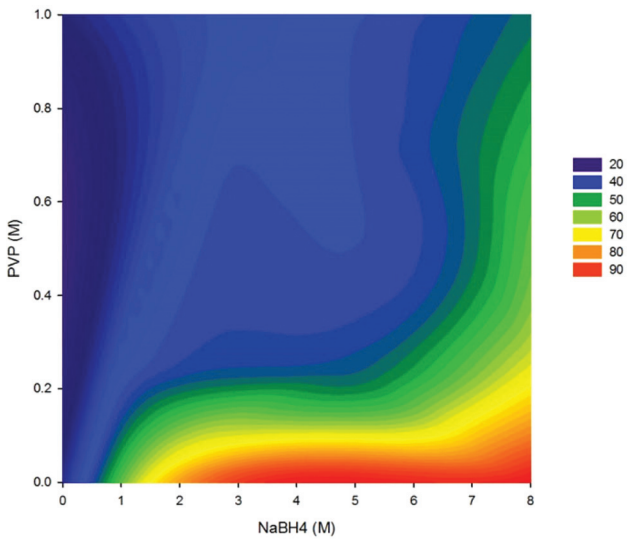

Fig. 7 Degree of crystallinity (%) of the nanoparticles as a function of PVP and $NaBH_4$ moles.

Conclusions

In this study, Sn-3.8Ag-0.7Cu nanosolders have been synthesized *via* a chemical reduction technique by employing PVP as a surfactant agent.

The findings of this investigation can be summarized as follows:

- The as-synthesized nanoparticles were comprised of an inner core of crystalline β-Sn, surrounded by an amorphous shell. It is proposed, that the shell consisted of several amorphous sublayers.
- Particle size drastically decreased by introducing PVP to the precursors, while a further increase in the amount of PVP altered the particle size only slightly.
- Competing reactions of the metal cations with PVP and OH^- groups in the solution form an amorphous tin hydroxyl gel around the metallic particles which itself is surrounded by a protective PVP layer.
- A melting point depression of 26.6 °C could be achieved for the nanoparticles with the average diameter of 18 nm.

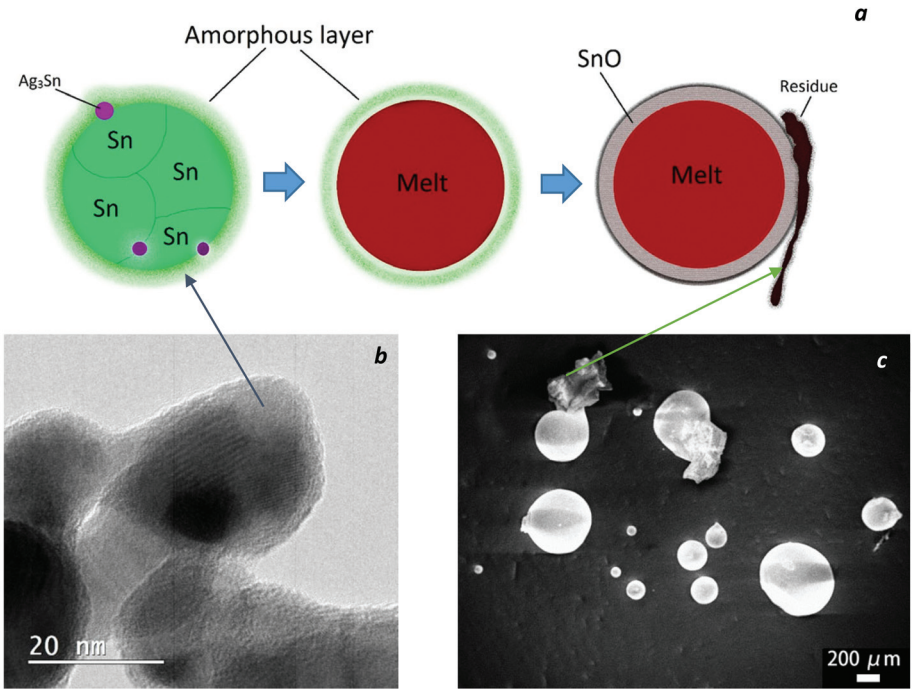

Fig. 8 (a) Schematic model of the structural and morphological evolution of SAC nanoparticles upon heating, (b) TEM image of the synthesized nanopowders and (c) SEM image of the same sample after heating cycle at 650 °C.

• During the process of annealing at a temperature slightly above the melting temperature of the SAC solder, the amorphous layer transforms to a crystalline SnO phase which, at a higher temperature, decomposes into Sn and SnO_2 in a disproportionation reaction. The observed exothermic signal around 260 °C could be an indicator for the rearrangement of the tin atoms that lead to the consolidation of the tin hydroxide/oxide structure and its crystallization.

Acknowledgements

Financial support for this study came from the Austrian Science Fund (FWF) under project nos. P26304 and P27049. The authors also want to acknowledge the help of Prof. V. Arion with the FTIR measurements and Mag. J. Theiner with the chemical CNH analyses as well as the support of Dr St. Puchegger with the SEM studies. TEM investigations were carried out using the facilities at the University Service Center for Transmission Electron Microscopy at the Vienna University of Technology.

Notes and references

1 K. Sim and J. Lee, Phase stability of Ag–Sn alloy nanoparticles, *J. Alloys Compd.*, 2014, **590**, 140–146.
2 T. Bachels and H. Güntherodt, Melting of Isolated Tin Nanoparticles, *Phys. Rev. Lett.*, 2000, **85**, 1250–1253.
3 C. Y. Lin, U. S. Mohanty and J. H. Chou, Synthesis and characterization of Sn–3.5Ag–XZn alloy nanoparticles by the chemical reduction method, *J. Alloys Compd.*, 2009, **472**, 281–285.
4 H. Jiang, K. Moon and C. P. Wong, Recent advances of nanolead-free solder material for low processing temperature interconnect applications, *Microelectron. Reliab.*, 2013, **53**, 1968–1978.
5 L.-Y. Hsiao and J.-G. Duh, Synthesis and Characterization of Lead-Free Solders with Sn-3.5Ag-xCu (x = 0.2, 0.5, 1.0) Alloy Nanoparticles by the Chemical Reduction Method, *J. Electrochem. Soc.*, 2005, **152**, J105–J109.
6 S. Pang and K. Yung, Green Approach to Synthesis of Nanoparticles of Sn3.0Ag0.5Cu Lead-Free Solder Alloy, *Mater. Trans.*, 2012, **53**, 1770–1774.
7 F. Frongia, M. Pilloni and A. Scano, Synthesis and melting behaviour of Bi, Sn and Sn–Bi nanostructured alloy, *J. Alloys Compd.*, 2015, **623**, 7–14.
8 J. Sopousek, J. Vrestal, A. Zemanova and J. Bursik, Phase Diagram Prediction And Particle Characterisation Of Sn-Ag Nano Alloy For Low Melting Point Lead-Free Solders, *J. Min. Metall., Sect. B*, 2012, **48B**(3), 419–425.
9 M. L. Lavcevic and Z. Ogorelec, Aggregates of Sn-clusters: partial coalescence during the initial heating, *Mater. Lett.*, 2003, **57**, 1885–1887.
10 R. Alcántara, U. Nwokeke, I. Rodríguez and J. L. Tirado, Electrochemical reaction of lithium with nanocrystalline $CoSn_3$, *Electrochem. Solid-State Lett.*, 2008, **11**, 209–213.
11 J. S. Thorne, P. P. Ferguson, R. D. Dunlap and J. R. Dahn, Effect of annealing on nanostructured Sn30Co30C40 prepared by mechanical attrition, *J. Alloys Compd.*, 2009, **472**, 390.

12 U. Nwokeke, F. Nacimiento, R. Alcntara and J. Tirado, FeSn 2-polyacrylonitrile electrode obtained by using high-intensity ultrasonication, *Electrochem. Solid-State Lett.*, 2011, **14**(10), 148–150.
13 M. J. N. V. Prasad and A. H. Chokshi, On the exothermic peak during annealing of electrodeposited nanocrystalline nickel, *Scr. Mater.*, 2011, **64**, 544–547.
14 P. Song and D. Wen, Experimental Investigation of the Oxidation of Tin Nanoparticles, *J. Phys. Chem. C*, 2009, **113**, 13470–13476.
15 K. C. Yung, C. M. T. Law, C. P. Lee, B. Cheung and T. M. Yue, Size Control and Characterization of Sn-Ag-Cu Lead-Free Nanosolders by a Chemical Reduction Proces, *J. Electron. Mater.*, 2012, **41**, 313–321.
16 Y. Gao, C. Zou, B. Yang, Q. Zhai, J. Liu, E. Zhuravlev and C. Schick, Nanoparticles of SnAgCu lead-free solder alloy with an equivalent melting temperature of SnPb solder alloy, *J. Alloys Compd.*, 2009, **484**, 777–781.
17 C. Zou, Y. Gao, B. Yang, X. Xia, Q. Zhai, C. Andersson and J. Liu, Nanoparticles of the Lead-free Solder Alloy Sn-3.0Ag-0.5Cu with Large Melting Temperature Depression, *J. Electron. Mater.*, 2009, **38**, 351–355.
18 C. Zou, Y. Gao, B. Yang and Q. Zhai, Melting and solidification properties of the nanoparticles of Sn3.5Ag0.5Cu lead-free solder alloy, *Mater. Charact.*, 2010, **61**, 474–480.
19 K.-W. Moon, W. J. Boettinger, U. R. Kattner, F. S. Biancaniello and C. A. Handwerker, Experimental and Thermodynamic Assessment of Sn-Ag-Cu Solder Alloys, *J. Electron. Mater.*, 2000, **29**, 1122–1136.
20 W. Zhang, C. Zou, B. Zhao, Q. Zhai and Y. Gao, Size control and its mechanism of SnAg nanoparticles, *Trans. Nonferrous Met. Soc. China*, 2014, **24**, 750–757.
21 M. Huh, S. Kim, J. Ahn, B. Kim and J. Park, Oxidation of nanophase tin particles, *Nanostruct. Mater.*, 1999, **11**, 211–220.
22 N. Wiberg, A. F. Holleman and E. Wiberg, *Holleman-Wiberg's Inorganic Chemistry*, Academic Press, New York, 1st edn, 2001.
23 R. Garrigos, P. Cheyssac and R. Kofman, Melting of lead particles of small sizes –influence of surface phenomena, *Z. Phys. D: At., Mol. Clusters*, 1989, **12**, 497–500.
24 W. Hu, S. Xiao, J. Yang and Z. Zhang, Melting evolution and diffusion behavior of vanadium nanoparticles, *Eur. Phys. J. B*, 2005, **45**, 547–554.
25 G. Carotenuto, G. P. Pepe and L. Nicolais, Preparation and characterization of nano-sized Ag/PVP composites for optical applications, *Eur. Phys. J. B*, 2000, **16**, 11–17.
26 T. M. Dung Dang, T. T. Tuyet Le, E. Fribourg-Blanc and M. C. Dang, The influence of solvents and surfactants on the preparation of copper nanoparticles by a chemical reduction method, *Adv. Nat. Sci.: Nanosci. Nanotechnol.*, 2011, **2**, 025004.
27 M. Sivakumar, S. Kanagesan, V. Umapathy, R. Suresh Babu and S. Nithiyanantham, Study of CoFe2O4 Particles Synthesized with Various Concentrations of PVP Polymer, *J. Supercond. Novel Magn.*, 2013, **26**, 725–731.
28 N.-L. Wu, S.-Y. Wang and I. A. Rusakova, Inhibition of Crystallite Growth in the Sol-Gel Synthesis of Nanocrystalline Metal Oxides, *Science*, 1999, **285**, 1375–1377.
29 R. Yang, Y. Gu, Y. Li, J. Zheng and X. Li, Self-assembled 3-D flower-shaped SnO2 nanostructures with improved electrochemical performance for lithium storage, *Acta Mater.*, 2010, **58**, 866–874.
30 P. Huang and J. Duh, Effects of Different Surfactant Additions and Treatments on the Characteristics of Tin Nanosolder by Chemical Reduction Method, *Electron. Compon. Technol. Conf.*, 2008, 431–435.
31 H. Uchiyama, Y. Shirai and H. Kozuka, Formation of spherical SnO_2 particles consisting of nanocrystals from aqueous solution of SnCl4 containing citric acid via hydrothermal process, *J. Cryst. Growth*, 2011, **319**, 70–78.
32 W. Brandt, F. Dwyer and E. Gyarfas, Chelate complexes of 1,10-phenanthroline and related compounds, *Chem. Rev.*, 1954, **54**, 959–1017.
33 C. Lo, K. Karan and B. Davis, Kinetic Studies of Reaction between Sodium Borohydride and Methanol, Water, and Their Mixtures, *Ind. Eng. Chem. Res.*, 2007, **46**, 5478–5484.